



Photocatalytic Degradation of 2,4-Dichlorophenol on NiAl-Mixed Oxides Derivatives of Activated Layered Double Hydroxides

Esthela Ramos-Ramírez¹ · Norma L. Gutiérrez-Ortega² · Francisco Tzompantzi-Morales³ · Arturo Barrera-Rodríguez⁴ · J. C. Castillo-Rodríguez³ · Clara Tzompantzi-Flores³ · Carlos E. Santolalla-Vargas⁵ · María del Pilar Guevara-Hornedo¹

Published online: 6 May 2020
© Springer Science+Business Media, LLC, part of Springer Nature 2020

Abstract

Advanced oxidation processes such as photocatalysis have assumed enormous importance in the scientific field as viable sustainable alternatives to be applied to the elimination of persistent organic pollutants present in water reservoirs for human consumption. Persistent organic compounds like pesticides that belong to the chlorophenol family are a global public health priority since they are associated with serious diseases like cancer and can even cause death at low concentrations of prolonged exposure. This work proposes the use of activated Ni/Al layered double hydroxides as photocatalysts for the degradation of 2,4-dichlorophenol. The study variables associated with the properties of the catalysts were the Ni/Al metal ratio as well as the synthesis conditions. To determine the structural properties of catalytic precursors and catalysts, the techniques of XRD, FTIR, UV-DR, DGTA, TPD, SEM-EDS and TEM were used. The photodegradation tests were carried out in a Bach type reactor with a high energy uv lamp. The results of the photocatalytic degradation of 2,4-dichlorophenol in aqueous solution showed good photocatalytic activity with a degradation efficiency of up to 94% attributed to the presence of Ni in the crystalline and amorphous structures of NiO–NiAl₂O₄ oxides by means of a combined oxidation-reduction mechanism due to the effect of holes and superoxide and hydroxyl radicals not associated with the memory effect of reconstruction of layered double hydroxides.

Keywords Photocatalysis · Layered double hydroxides · Coprecipitation · Chlorophenols · Photodegradation

1 Introduction

In recent years, the use of catalytic processes with semiconductors for the treatment of water for human and residual consumption has attracted attention in the field of research because they are sustainable processes of easy operation,

low cost, high efficiency and zero toxicity [1, 2]. The main advantage of these processes is that they can degrade persistent organic compounds through oxidation and reduction processes until they are mineralized according to the general reaction [3]:

✉ Esthela Ramos-Ramírez
ramosre@ugto.mx

✉ Norma L. Gutiérrez-Ortega
normagut@ugto.mx

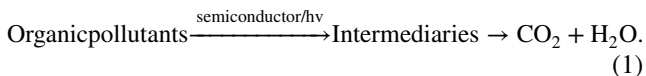
¹ Departamento de Química, División de Ciencias Naturales y Exactas, Campus Guanajuato, Universidad de Guanajuato, Noria Alta s/n, Col. Noria Alta, C.P. 36050 Guanajuato, GTO, Mexico

² División de Ingenierías, Departamento de Ingenierías Civil y Ambiental, Universidad de Guanajuato, Campus Guanajuato, Av. Juárez 77 Centro Histórico, C.P. 36000 Guanajuato, GTO, Mexico

³ Departamento de Química, Universidad Autónoma Metropolitana-Iztapalapa, Av. San Rafael Atlixco No. 189, C.P. 09340 Mexico, Mexico

⁴ Centro Universitario de la Ciénega de la Universidad de Guadalajara, Av. Universidad No. 1115, Col. Linda Vista, C.P. 47820 Ocotlán, JAL, México

⁵ Centro Interdisciplinario de Investigaciones y Estudios Sobre Medio Ambiente y Desarrollo (CIEMAD) Instituto Politécnico Nacional, Delegación Gustavo A. Madero, Calle 30 de Junio de 1520 s/n, Barrio la Laguna Ticomán, C.P. 07340 Ciudad de Mexico, Mexico



The main semiconductor material used as a photocatalyst has been the TiO₂ in anatase phase which is characterized by having a solitary electron in its last orbital which, upon receiving photonic energy (*hν*) of a prohibited band greater than or equal to 3.2 eV, is photoexcited to the band of conduction leaving a vacuum in the valence band, thus creating the electron-hole pair (*e*⁻ – *h*⁺) for nanoseconds. The presence of *e*⁻ sensors, such as oxygen, allows the formation of superoxide radicals (O₂⁻), said radical can be protonated to form the hydroperoxyl radical (HO₂⁻) and subsequently H₂O₂. H₂O₂ can inhibit recombination of the electron-hole pair, in addition to providing additional OH⁻ radicals [4]. On the other hand, the *h*⁺ gap favors the reduction of H₂O molecules allowing the formation of OH⁻ radicals [5], as shown in Fig. 1.

Since the discovery of the photocatalytic effect by water division using a TiO₂ electrode [6], numerous investigations have evolved towards the synthesis of the TiO₂ catalyst of different scales (nanometric, millimeter) and shapes (spheres, nanotubes, fibers, tubes, sheets), characterize their physical properties and determine their photooxidation yields to the nature of the surface of the photocatalytic reaction [7–9]. Other research has focused on the chemical modification of TiO₂ (doped with nanoparticles or particles with transition metals and lanthanides), or on the formation of composites with various organic and inorganic materials such as chitosan, chitin, polyoxytugstate, metal oxides (MnO₄, Fe₂O₃, SrTiO₃, ZnO, ZnFe₂O₃, etc.) [10–16]. Even combined advanced oxidation systems have been tested [17]. The emerging pollutants that have been studied for degradation through photocatalytic processes are pesticides (DDT, eldrin, chlorophenols, bromophos, malathion), as well as drugs such as acetaminophen, imidazole, ciprofloxacin), dyes such as rhodamine, acid orange, reactive

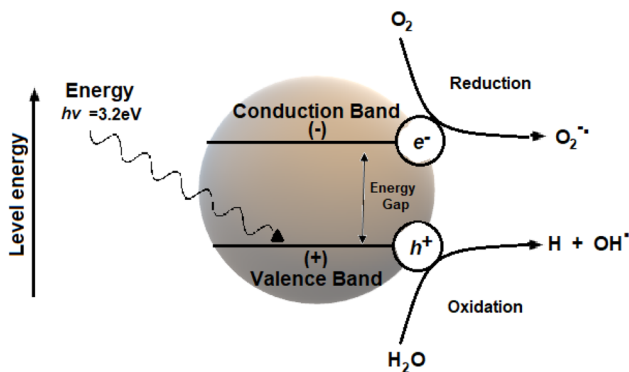


Fig. 1 Photo-induced formation mechanism of electron-hole pair in a semiconductor TiO₂

red, methylene blue), among others [18–20]. Phenolic compounds are a family of compounds that are characterized by having a hydroxyl group attached to the phenyl ring, which are mostly listed by the EPA as a priority to control their exposure [21–24]. One of the compounds derived from phenol is 2,4-trichlorophenol (2,4-DCP), which is considered non-biodegradable, toxic, volatile and highly corrosive. At low concentrations, 2,4-DCP causes great damage to organisms and the environment, and its massive accumulation in humans can cause carcinogenesis, teratogenesis and death. 2,4-DCP can be found in drinking water and wastewater, as well as in soils, as a result of its use as a pesticide, herbicide, preservative, among others, or as products of the degradation of chemicals in the paper industry, agricultural and food [25–27].

Layered double hydroxides are hydrated anionic clays, with semiconductor properties that make them promising materials for application in photocatalysis [28]. Its semiconductor properties are attributed to its composition and chemical structure, consisting of divalent and trivalent intercalated metal cations (M²⁺ = Mg²⁺, Ca²⁺, Zn²⁺, Co²⁺, Ni²⁺; M³⁺ = Al³⁺, Cr³⁺, Fe³⁺, among others) in the center of octahedra with vertices occupied by hydroxyls; octahedral structures line up in positively charged layers; and the load is compensated by anions housed in the interlaminal space (Aⁿ⁻ = CO₃²⁻, NO₃⁻, SO₄²⁻, Cl⁻, among others), resulting in the general mineralogical formula, [M²⁺_{1-x}M³⁺_x(OH)₂]^{x+}(Aⁿ⁻)_{x/n}·mH₂O (Fig. 2). One of the characteristic properties of layered double hydroxides is that they are heat treated and generate photoresistant semiconductor nanocomposites consisting of mixtures of single and double metal oxides with high surface area and good crystallinity [29–31].

The most studied double laminar hydroxides are those consisting of Mg²⁺, Al³⁺ and CO₃²⁻, which make up the mineralogical structure of the hydrotalcite Mg₆Al₂(OH)₁₆CO₃·4H₂O [32–34], which have reported the degradation capacity of compounds persistent organics such as phenols and their derivatives. Recent research is focusing on the design and synthesis of these materials composed of transition metals, mainly Zn, Fe, Co, Cr and even Cu, with the aim of improving their properties and degradability, until complete mineralization [35–37]. Few studies have focused on the incorporation of Ni, which is a strong reducing agent,

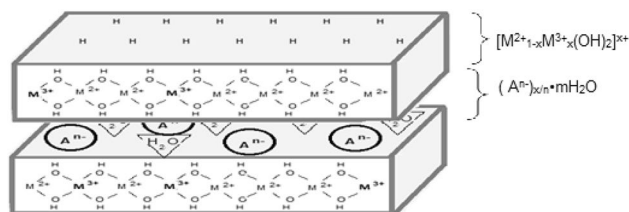


Fig. 2 Layered double hydroxides structure

which can help the generation of chemically active sites for photodegradation, considering that in studies conducted with metal nanoparticles containing Ni photocatalytic activity is improved [38–40]. Recent applications have been given to Ni-containing layered double hydroxides for catalytic processes, energy storage, among others [41–42].

In the present work it is proposed to obtain layered double hydroxides with different Ni/Al metal ratio, 2 and 3 by the coprecipitation method, to identify the effect of the amount of Ni on the catalyst structure. Additionally, it is compared with a Ni/Al catalyst of ratio 3 obtained at different pH to identify the effect on the generation of catalytically active sites. The photocatalytic capacity of synthesized materials is tested using as a model molecule degradation of persistent organic compounds to 2,4-dichlorophenol.

2 Materials and Methods

2.1 Obtaining Photocatalysts

The double Ni/Al layered double hydroxides of ratio 2 and 3 were obtained by the coprecipitation method to be used as catalytic precursors. The Ni/Al layered double hydroxide hydroxide of molar ratio of 2 was obtained by coprecipitating a solution with 1 mol of nickel nitrate hexahydrate (JT Backer) and 1 mol of nitrate of aluminum nonahydrate (JT Backer), with a basic solution of 1M sodium hydroxide (JT Backer). Coprecipitation was carried out at a pH of 11.5. The precipitated gel was washed to a pH of 9 and then dried at 100 °C to obtain the solid identified as HTC2N. The layered double hydroxide of Ni/Al ratio = 3 was obtained with the same methodology but varying the molar amount of each of the nickel and aluminum sources to obtain the desired ratio. The solid obtained was identified as HTC3N. Finally, a third layered double hydroxide of molar ratio Ni/Al = 3 was synthesized using the same methodology, except that the solid precipitated at a pH of 12.6 and the washings were performed until a pH of 10 was reached. The solid was identified as HTCC3N. For the activation of the layered double hydroxides, the synthesized solids were heat treated at 450 °C in an air atmosphere for 4 h for the formation of Ni/Al mixed oxides and were identified as HTC2N-450 °C, HTC3N-450 °C and HTCC3N-450 °C.

2.2 Physicochemical Characterization of Catalytic Precursors and Catalysts

For the X-ray diffraction analysis for the identification of the crystalline phases, an INEL Equinox Powder Diffractometer device with copper anode and $\text{CuK}\alpha$ monochromatic radiation with a wavelength of 1.5418 Å was used. The infrared spectra for the identification of the interlaminar anions

and the links of the laminar structures, were obtained in an infrared spectroscope with Perkin-Elmer 1600 series Fourier transforms in a wave number region of 1000 to 4000 cm^{-1} . The thermal evolution profiles by thermogravimetric analysis and differential thermal analysis were determined in a TA Instruments Thermo-Analyzer at a heating rate of 10 °C/min in an air atmosphere at a speed of 100 mL/min and using α -alumina as reference standard. The qualitative and quantitative composition as well as the chemical states of the elements on the surface of the matter was determined using X-ray photoelectronic spectroscopy, which was run using a Thermo Fisher scientific spectrophotometer with a monochromatic $\text{AlK}\alpha$ radiation (1486.6 eV) with a source X-ray and was micro-focused to the source obtaining a spot size on the sample of 400 microns in diameter. To compensate for the effect related to the turn changes, the C 1s peak at 284.6 eV was used as an internal standard. To verify the optimal working range of solids as photocatalysts, UV-Vis spectra were determined by diffuse reflectance spectroscopy in a Perkin-Elmer lambda UV-Vis-NIR spectrophotometer. The banned band energy (e.g.) of the samples was calculated from the ultraviolet absorption spectra of diffuse reflectance, considering that $e.g. = (1239b/\alpha)$, where α and b are coefficients that were linearized in the region appropriate spectrum. The programmed temperature desorption technique (TPD), using the CO_2 probe molecule, was applied to determine the density and strength of the basic centers in mixed oxides in a BelCat model TPD/TPR/TPO analyzer Bel Japan Brand kit. The elemental and surface mapping were performed in a surface electron microscope with a X-ray dispersive energy spectroscopy (SEM-EDS) microwave, performed in a scanning electron microscope, model Supra 55VP, Carl Zeiss brand. Elemental analysis (SEM/EDS) with an Oxford Instruments brand detector. High resolution electron microscopy (HRTEM) was performed on a JEOL 2100F electron microscope, equipped with a GATAN ($\pm 22^\circ$) double tilt goniometer stage. Furthermore, the HRTEM FFT image analysis was performed with the Digital Micrograph software program.

2.3 Evaluation of Photocatalytic Activity in the Degradation of 2,4-Dichlorophenol

The photocatalytic degradation capacity of 2,4-dichlorophenol using the catalysts obtained, was determined under the following conditions: 200 mL standard solution of 2,4-dichlorophenol (Aldrich) at a concentration of 40 ppm, in a temperature controlled Batch reactor of 25 °C with constant magnetic stirring of 700 rpm, with an air flow of 2 mL/s and an irradiation of UV light of 254 nm and an emission of 2.5 mW/cm^2 generated by a Pen-Ray UV lamp inserted into a quartz tube. Prior to uv irradiation, the catalyst was contacted with the standard solution of 2,4-dichlorophenol for a

period of 1 h in the dark to verify an adsorption-desorption equilibrium of the contaminating molecule with the catalyst. Once the equilibrium was reached, irradiation began for a period of 2 h. In addition to the comparison against a reference photocatalyst, commercial TiO₂-P25 was used. In all cases, the process of degradation of the contaminant was monitored by sampling aliquots of the reactor, with the subsequent quantification of this in a Cary 100 UV–Vis spectrophotometer at a wavelength of 283 nm.

2.4 Hydroxyl and Superoxide Radical's Detection and Hole Trap Study

To quantify hydroxyl radicals, (OH[•]) generated by the photocatalyst during photocatalytic degradation, the technique based on the formation of 7-hydroxycoumarin was used, which was followed by Fluorescence Spectroscopy on a SCINCO FS-2 spectrometer. A diluted aqueous solution (2×10^{-3} M) of coumarin was prepared, 200 mL of solution was poured into a Batch reactor and 200 mg of photocatalyst to be analyzed, and TiO₂-P25 was used as reference material. Similarly, the study was conducted in the absence of photocatalyst (photolysis) to observe the possible production of hydroxyl radicals with and without photocatalyst. Subsequently, the solution was irradiated with UV light for 1 h with a Pen-Ray lamp ($\lambda = 254$ nm and $I_0 = 4.4$ mW cm⁻²), with constant stirring, oxygen bubbling and temperature conditions (800 rpm, 1 mL s⁻¹) 25 °C respectively) by extracting 3 mL aliquots at five minute intervals. Finally, the fluorescence emission spectra in the irradiated solution were analyzed by photoluminescence, at a wavelength of 320 nm. The determination of the influence of the absence of bubbled oxygen and therefore, absence of superoxide radicals (reaction bubbled with nitrogen) was carried out. In this test 200 mg of photocatalyst and 200 mL of 2,4-dichlorophenol solution were used at 40 ppm with a nitrogen flow of 1 mL s⁻¹. The reaction was carried out for 2 h by extracting aliquots in a 15 min interval.

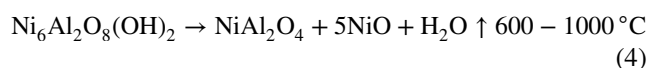
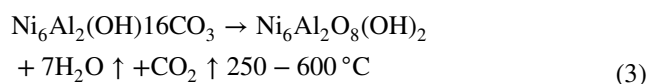
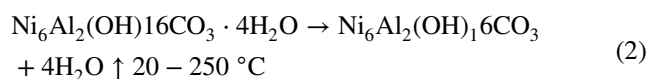
3 Results and Discussion

3.1 Differential and Gravimetric Thermal Analysis

The thermal decomposition of the layered double hydroxides depends to a great extent on the nature of the cations that form the sheets and on the interlaminar anions as well as on the experimental conditions of synthesis [43]. The thermal evolution profiles of the catalytic precursors are shown in Fig. 3, corresponding to the differential and gravimetric thermal analysis for the catalysts HTC2N (Fig. 3a), HTC3N (Fig. 3b) and HTCC3N (Fig. 3c). As can be seen for the solid HTC2N and HTC3N the decomposition is similar, occurring

in two stages [44]. The first loss corresponds to the release of interlaminar water with endothermic peaks between 20 and 185 °C for the solid HTC2N, and between 20 and 232 °C for HTCC3N, losing 13.5 and 13.2% of its weight, respectively. The second stage associated with a second endothermic peak that starts from the end of the first and ends at 500 °C for the solid HTC2N and HTC3N with a total loss of 40.5 and 37.3%. Analyzing the second loss in more detail, it can be seen that for the HTC2N solid it is the result of the superposition of two signals, their maximums being located at 280 °C and 310 °C associated with different crystalline phases present in the precursor and which undergo thermal evolution, at It differs from the HTC3N solid which is a single signal associated with a pure solid with a single thermal decomposition presenting a simultaneous decarbonization and dehydroxylation with which simple and mixed metal oxides are formed. Finally, at 825 °C a small endothermic peak is observed associated with the evolution of the amorphous mixed Ni–Al oxide to a crystalline phase without weight loss. In the case of the solid HTCC3N, a first stage of dehydration below 200 °C of 17% and a second weight loss of 250 to 600 °C of 16.5% of the partial elimination of carbonates and hydroxyl and a third loss are observed. additional 14% from 600 to 700 °C corresponding to the carbonates that remained occluded in the structure of the calcined solids, reaching a total loss of 44.3%. The above is attributed to the very basic pH of synthesis that favored the formation of additionally segregated hydroxides to the Ni/Al layered double hydroxides.

The general reactions associated with the thermal decomposition of the synthesized solids are shown in Eqs. 2, 3 and 4 where you can see the crystalline and amorphous phases that form during the process.



Based on the decomposition process of the solids, the calcination of the solids at 450 °C is proposed for their activation as catalysts formed by a mixture of simple and mixed oxides.

3.2 X-ray Diffraction

The diffraction patterns of the catalytic precursors (HTC2N, HTC3N and HTCC3N), of the catalysts before photodegradation (HTC2N-450 °C, HTC3N-450 °C and

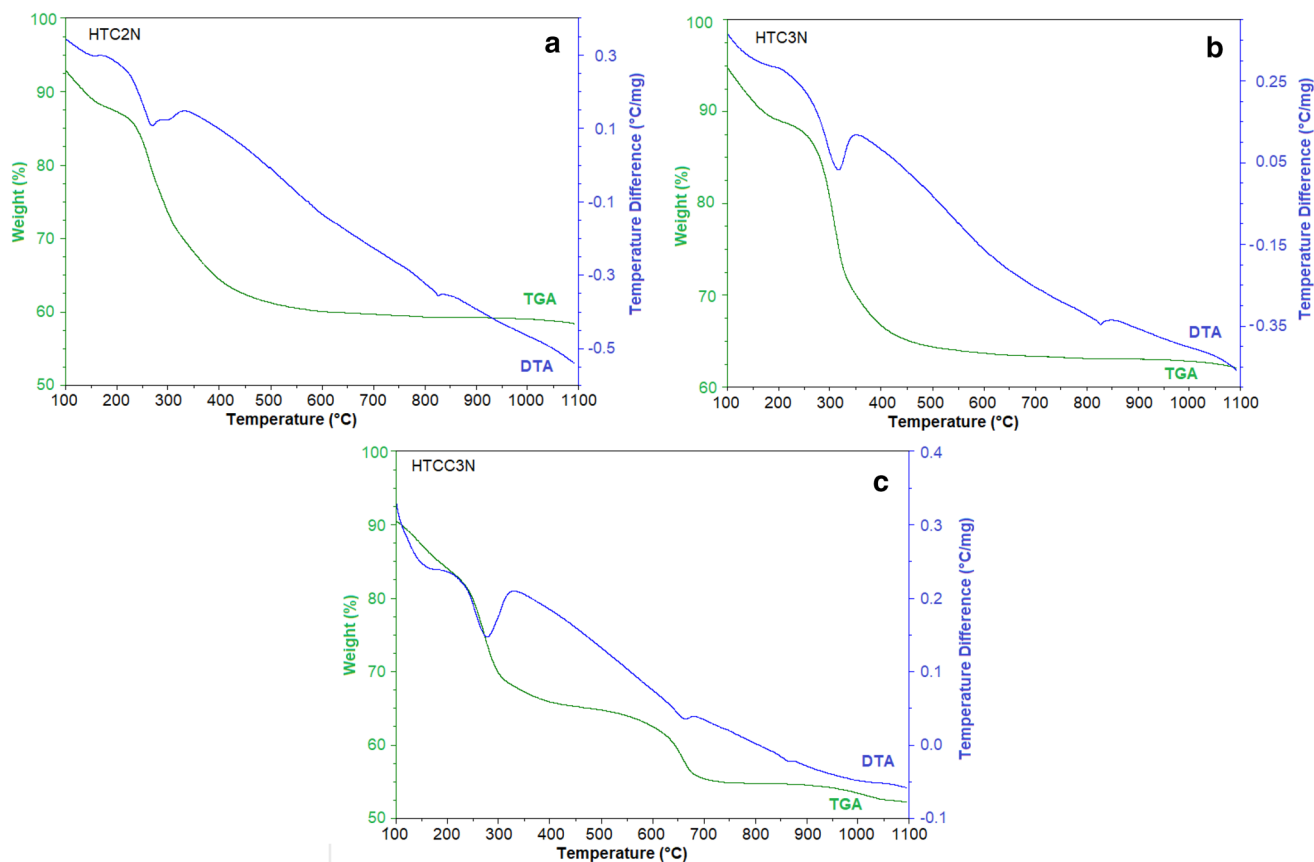


Fig. 3 Differential and gravimetric thermal analysis of the **a** HTC2N, **b** HTC3N and **c** HTCC3N catalysts

HTCC3N-450 °C) and after photodegradation (HTC2N-450 °C-P, HTC3N-450 °C-P and HTCC3N-450 °C-P) are shown in Fig. 4. As can be seen, the patterns of the precursors are very similar to each other, as are the patterns of the catalysts before and after photodegradation. With respect to the catalytic precursors (Fig. 4a), the characteristic signals at angles 2θ of 13.0, 23.0, 36.0, 38.7, 46 and 61 could be identified by the Miller indices (003), (015), (110), (1013), (0116) and (2014) respectively, corresponding to the takovite phase hydroxalcite according to card 00-015-0087 JCPDS. The most significant differences between the different synthesized solids have to do with the crystallinity and purity of the crystalline phases. Comparing the HTC2N solids with the HTC3N, the solid with a Ni/Al = 3 metal ratio shows better crystallinity and higher purity when showing only the takovite signals. The Ni/Al = 2 ratio solid has the crystalline phase of takovite but is less crystalline than the ratio 3 solid, in addition to containing a Ni(OH)₂ crystalline phase from the JCPDS 14-0117 card, with peaks in narrow and high intensity at 19°, 22° and 43° theta, which was formed at the time of synthesis due to the presence of a greater Ni molar in the solution at the pH of 11.5. Regarding the solid HTCC3N,

it can be seen that it is the solid with the highest crystallinity, however, at a pH of 12.6 of precipitation, the formation of a crystalline phase of the NiAl₂O₄ spinel was favored with narrow peaks at 22, 31, 47 and 67 theta degrees according to JCPDS card 10-0339. This indicates that the best conditions to obtain a Ni/Al layered double hydroxides is with a Ni/Al = 3 molar ratio at a synthesis pH of 11.5 and washes up to a pH of 9.

Figure 4b shows the diffraction patterns of the solids calcined at 450 °C before the photodegradation process, where for the 3 solids the crystalline phase of NiO is predominantly observed. For the HTC2N and HTC3N solids only the phase of low crystallinity NiO is observed with signals at 38, 43, 64, 78 and 80 θ°, corresponding to the Miller indices of the planes (111), (200), (220), (311) and (222) respectively corresponding to the JCPDS card 00-047-1049. This suggests that the NiO phase was secreted at the thermal decomposition of the layered double hydroxides, and that the NiAl₂O₄ spinel is in the amorphous phase [45]. With respect to the HTCC3N solid calcined at 450 °C, it is possible to observe, in addition to the NiO crystalline phase, the presence of a NiAl₂O₄ crystalline phase which is present from the moment of

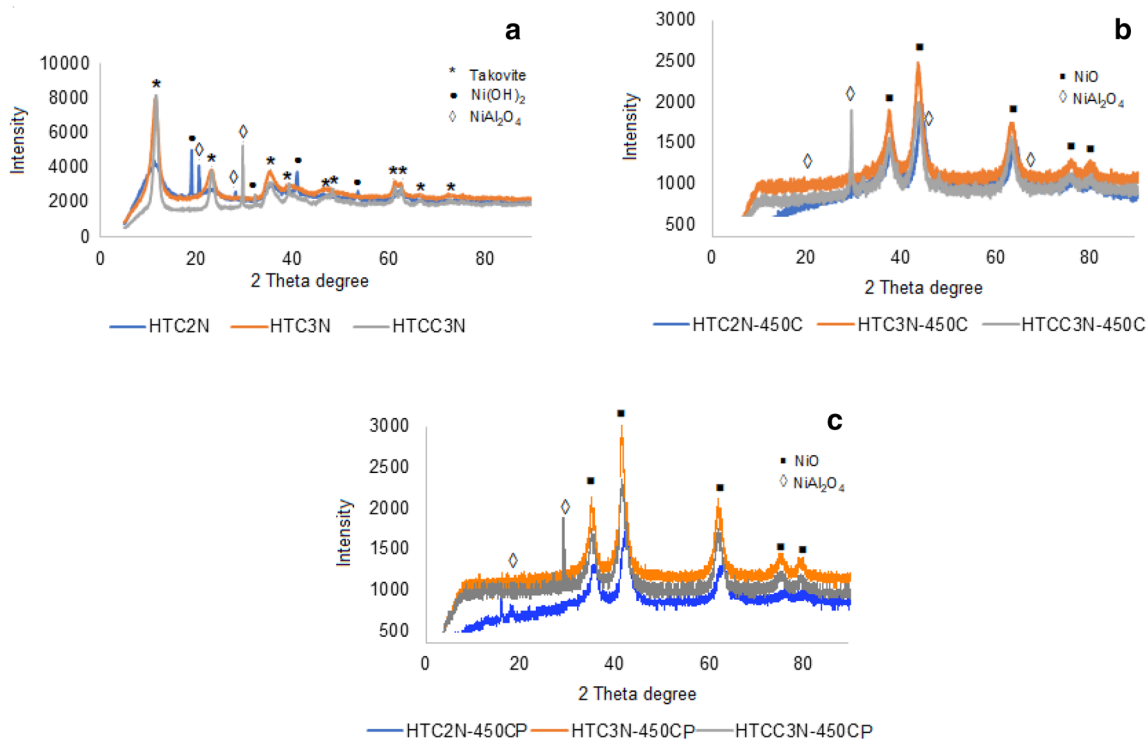


Fig. 4 X-ray diffraction patterns: **a** Ni/Al layered double hydroxides synthesized, **b** Ni/Al layered double hydroxides calcined at 450 °C before photodegradation and **c** Ni/Al layered double hydroxides calcined at 450 °C after photodegradation

synthesis. The diffraction patterns of the solids at 450 °C confirm that the layered double hydroxide have evolved into a mixture of potentially photocatalytically active single and Ni/Al mixed oxides.

Figure 4c shows the diffraction patterns of the catalysts after the photodegradation process. It is observed that once the photocatalytic reaction has been carried out, the materials do not have the so-called memory effect, since the characteristic planes of (b) and (c) are preserved, maintaining the structure of simple mixed oxides. The above would suggest

that the catalytic activity is not due to the memory effect, but to the presence of mixed and simple oxides catalytically active in the degradation of 2,4-dichlorophenol.

3.3 Infrared Spectroscopy with Fourier Transforms (FTIR)

In Fig. 5, the FTIR spectra of the Ni/Al layered double hydroxides and calcined at 450 °C are shown. In the different synthesized layered double hydroxides (Fig. 5a), a

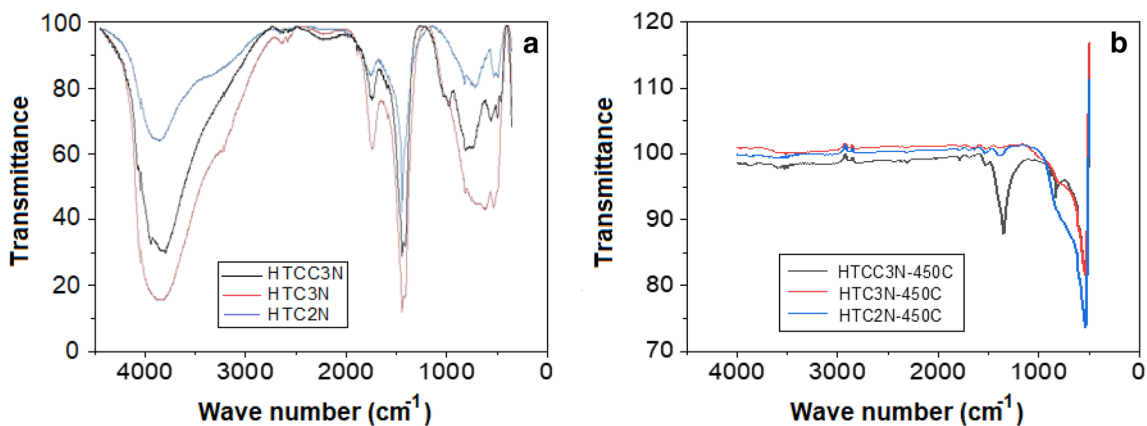


Fig. 5 Infrared spectra of HTC3N, HTC3N and HTCC3N photocatalysts **a** synthesized and **b** treated at 450 °C

characteristic band at 3400 cm^{-1} is distinguished, attributed as the OH stretch band of the hydroxyl-metal groups and of the vibration of the hydroxyl of the interlaminar water molecules that phase the band at 3200 cm^{-1} due to the vibration between them and the other interlaminar anions. A small band centered approximately 1630 cm^{-1} is due to the bending vibration of the water molecules. Furthermore, the band at 1384 cm^{-1} can be assigned to the vibration of CO_3^{2-} ions present in the interlayer layer. For HTCC3N solids, the presence of NO_3^- ions with a small characteristic band at 975 cm^{-1} is observed. Vibration signals below 850 cm^{-1} correspond to M–O, M–O–M vibrations [45–47]. For vibrations in layered double hydroxides, these vibrations are merged into a wide band of 833 to 595 cm^{-1} by the Ni–O, Ni–O–Ni, and Ni–O–Al vibrations, as seen in the HTC3N solid. The presence of Ni–OH and NiAl_2O_4 could be verified with the definition of the bands centered around 800 and 600 cm^{-1} .

For layered double hydroxides calcined at $450\text{ }^\circ\text{C}$ (Fig. 5b), all three spectra can be seen that the signals are similar in position but vary in intensity. From 4000 to 1600 cm^{-1} there are no significant signals that could be attributed to the presence of OH groups and to water molecules present in the catalytic precursors. Only from 1600 to 400 cm^{-1} are all the significant signs found. The above confirms the presence of simple and mixed metal oxides in a range below 1000 cm^{-1} for vibrations Al–O, Ni–O, O–Al–O, O–Ni–O. Specifically the vibration frequency of 590 cm^{-1} is attributed to the Al–O link, the band at 630 cm^{-1} corresponds to the O–Al–O vibration and the band at 648 cm^{-1} to the Ni–O vibration. Comparing the signals of the solid HTC2N with the HTC3N, it is observed that the solid HTC2N have a wide band of 600 to 900 cm^{-1} that corresponds to a greater amount of O–Ni–O vibrations due to the excess of Ni in the solid. While comparing the solid HTC3N with the HTCC3N it can be seen that it shows an intense signal centered at 1360 cm^{-1} that is attributed to the presence of remaining carbonate ions in the structure given its affinity for the oxides present which, as can be seen in thermogravimetric analysis is eliminated between 300 and $600\text{ }^\circ\text{C}$.

3.4 X-ray Photoelectron Spectroscopy (XPS)

Figure 6a shows the XPS study of the HTC2N photocatalyst, showing the signals attributed to the presence of Al, C, Ni and O. With respect to the species present in Al, it was found that the Gaussian components for Al $2p$ show peaks Al $2p_{3/2}$ and Al_2 at 75.69 , 73.68 , 70.65 , 67.82 and 62.85 eV , which corresponds to metallic Al species and Al oxide. For Ni species, Ni $2p_{1/2}$ and Ni $2p_{3/2}$ at 879 , 872 , are also shown. 861 and 855 eV corresponding to the species Ni $(\text{OH})_2$, Ni $(\text{OH})_2$ and NiO. With respect to the presence of O, C $1s$ peaks at 531.27 and 529.76 eV were identified, corresponding to the H–O–C and C–O species attributed to the

interaction of the interlaminar carbonate ions with the laminar structures of the layered double hydroxides; and finally with respect to the C signals, the O $1s$ signals were found at 289.79 , 288.83 , 285.08 and 284.64 associated to O–C=O, O–C=O, C–O–C and C–C respectively, of the interlaminar carbonates.

Figure 6b shows the XPS study of the HTC2N- $450\text{ }^\circ\text{C}$ photocatalyst, where the presence of Al, C, Ni and O is observed. Gaussian components for Al $2p$ show peaks 76.63 , 73.89 , 70.46 and 67.98 eV which corresponds to metal and oxide. For Ni $2p_{1/2}$, peaks 879.77 , 873.57 , 861.85 and 863.03 of the species Ni $(\text{OH})_2$ and NiO, Peaks C $1s$ at 284 , 286 and 288 eV , corresponding to C–C, C–O–C and O–C=O bonds, can be seen. O $1s$ at 533 and 531 eV corresponding to H–O–C and C–O links are also shown.

Comparing the HTC2N solid with the solid calcined at $450\text{ }^\circ\text{C}$, the significant differences focus on the predominance of the metal oxide species in the calcined solids, as well as the dehydroxylation and decarbonation of the layered double hydroxides.

The XPS spectra of the HTCC3N photocatalyst are shown in Fig. 6c, where the presence of Al, C, Ni and O is also observed. The Gaussian components for Al $2p$ show Al $2p_{3/2}$ and Al_2 peaks at 76 , 73 , 69 and 68 eV , which corresponds to the species Al Oxide and Al Metal. Ni $2p_{1/2}$ and Ni $2p_{3/2}$ are also shown at 879 , 873 , 861 and 855 eV corresponding to the species Ni $(\text{OH})_2$, Ni $(\text{OH})_2$ and NiO.

Figure 6d shows the XPS spectra of the HTCC3N- $450\text{ }^\circ\text{C}$ photocatalyst where the presence of Al, C, Ni and O is observed. Gaussian components for Al $2p$ show C $1s$ peaks at 288 , 286 and 284 eV , corresponding to OC links = O, COC and CC, Y. O $1s$ are also shown at 536 , 531 and 529 eV corresponding to HOC and CO links.

3.5 Diffuse Reflectance Spectroscopy

The evaluation of the bandgap energy (e.g.) for activated layered double hydroxides was calculated using the Kubelka–Munk equation [$F(R) = (1 - R)/2R$], extrapolating the absorption edges towards $F(R) = 0$ where R is the converted reflectance (%) of the UV absorption spectra, and are reported in Fig. 7 [48]. The solid HTC2N shows a bandgap slightly less than that of the HTC3N with values of 2.81 and 2.89 eV attributed to the fact that the solid HTC2N contains a greater amount of Ni, so it favors the semiconductor property. Comparing the banned band energy of HTC3N and HTCCN3 solids, a solid obtained at a higher pH has a slightly higher energy with values of 2.96 eV due to the segregation of aluminum, reducing semiconductor capacity. By comparing these prohibited band energy values and comparing them with the energy

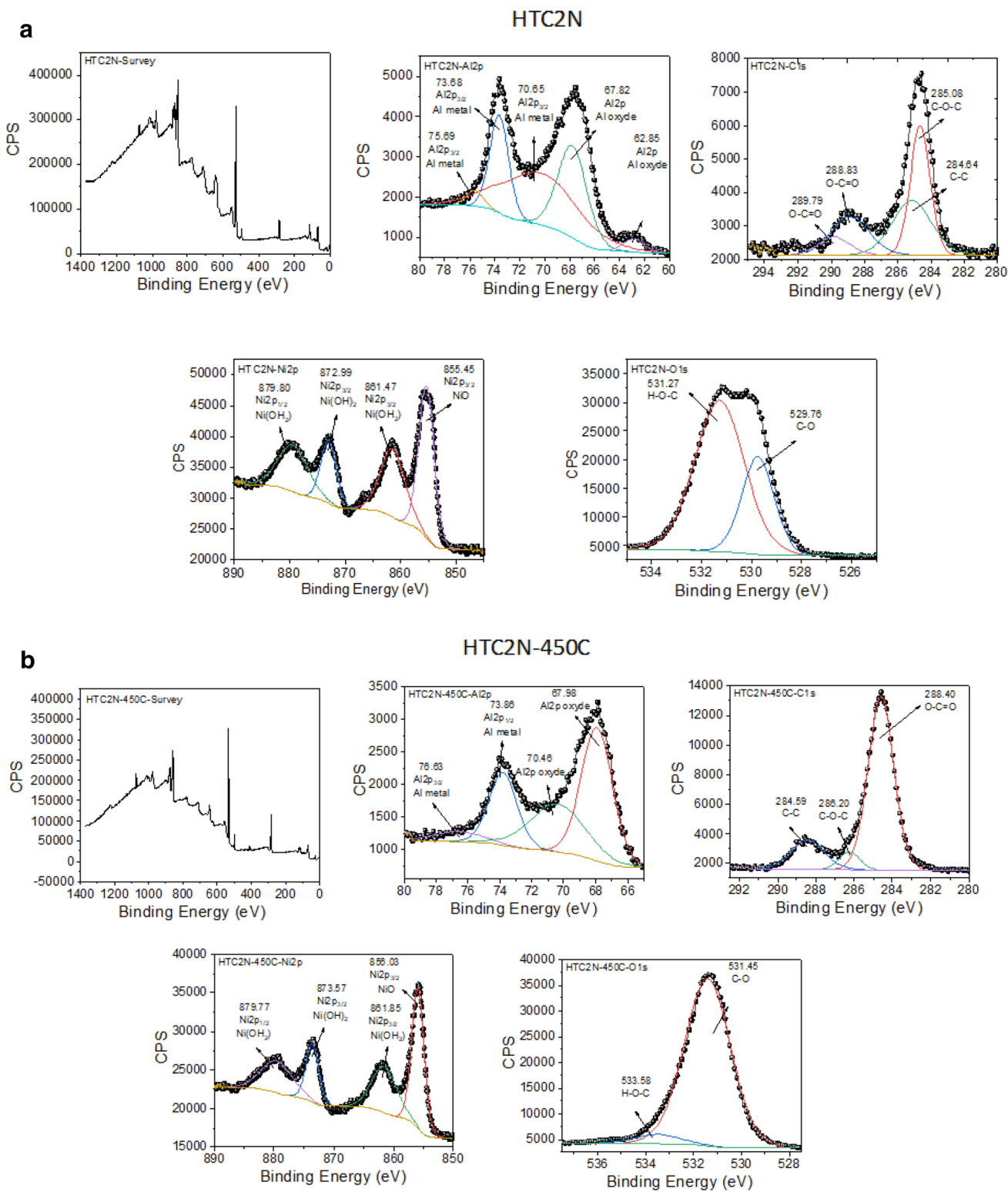


Fig. 6 a X-ray photoelectron spectroscopy (XPS) of the HTC2N photocatalyst. **b** X-ray photoelectron spectroscopy (XPS) of the HTC2-450 °C photocatalyst. **c** X-ray photoelectron spectroscopy (XPS) of

the HTCC3N photocatalyst. **d** X-ray photoelectron spectroscopy (XPS) of the HTCC3N-450 °C photocatalyst

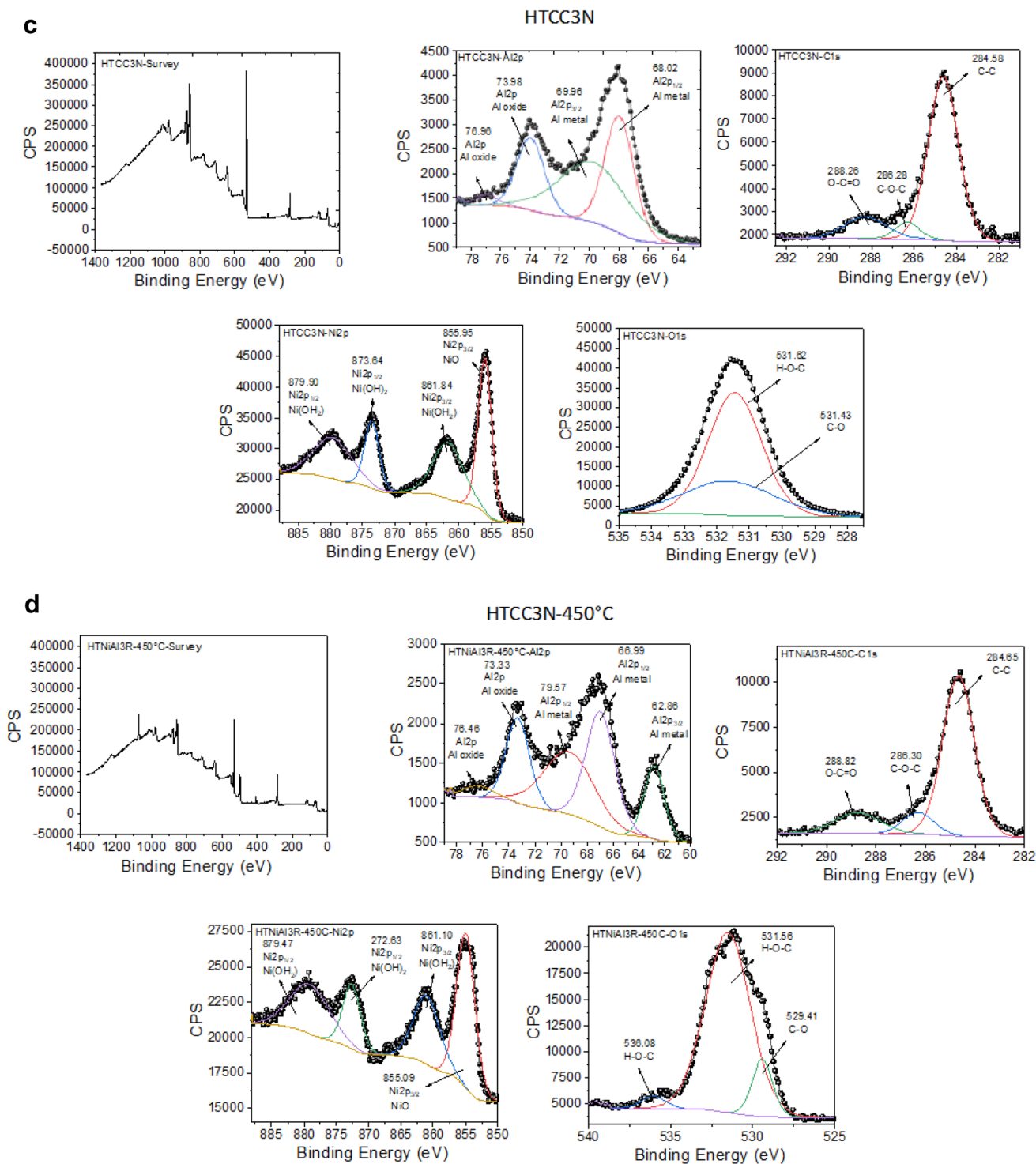


Fig. 6 (continued)

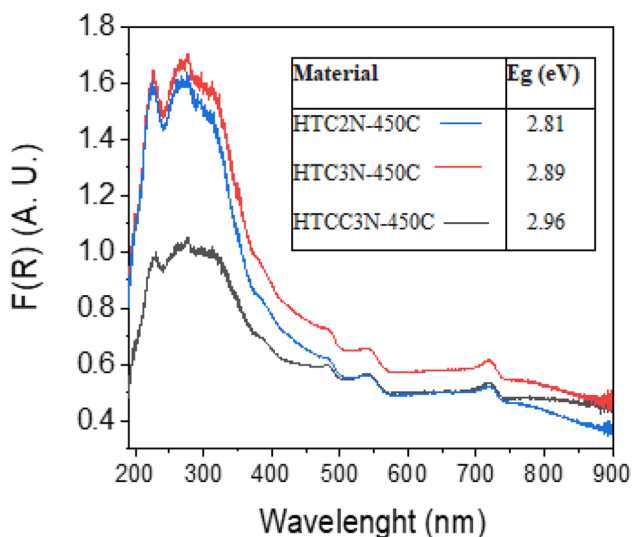


Fig. 7 UV–Vis–KM spectra (Kubelka–Munk Method) for Ni/Al activated layered double hydroxides

of TiO_2 -P25, with values of 3.20 eV for the anatase phase, Ni/Al layered double hydroxides are potentially competitive semiconductors with respect to TiO_2 -P25.

3.6 Evaluation of the Photocatalytic Degradation of 2,4-Dichlorophenol in Aqueous Solution

Figure 8 shows the ultraviolet–visible spectra of the 40 ppm degradation of 2,4-Dichlorophenol as a function of time, using activated catalysts HTC2N, HTC3N, HTCC3N and TiO_2 as reference control as a photocatalyst. The characteristic spectrum of 2,4-dichlorophenol has three characteristic absorption bands, the primary transition attributed to the aromatic group, the secondary transition due to the aromatic group and the $n \rightarrow \pi^*$ transition attributed to the C–Cl bond, centered at 210.5, 245 and 283 nm respectively. The degradation spectra of 2,4-Dichlorophenol using the catalysts show how these three bands show modifications and phase shifts associated with the degradation of the contaminant and the formation of intermediates [49].

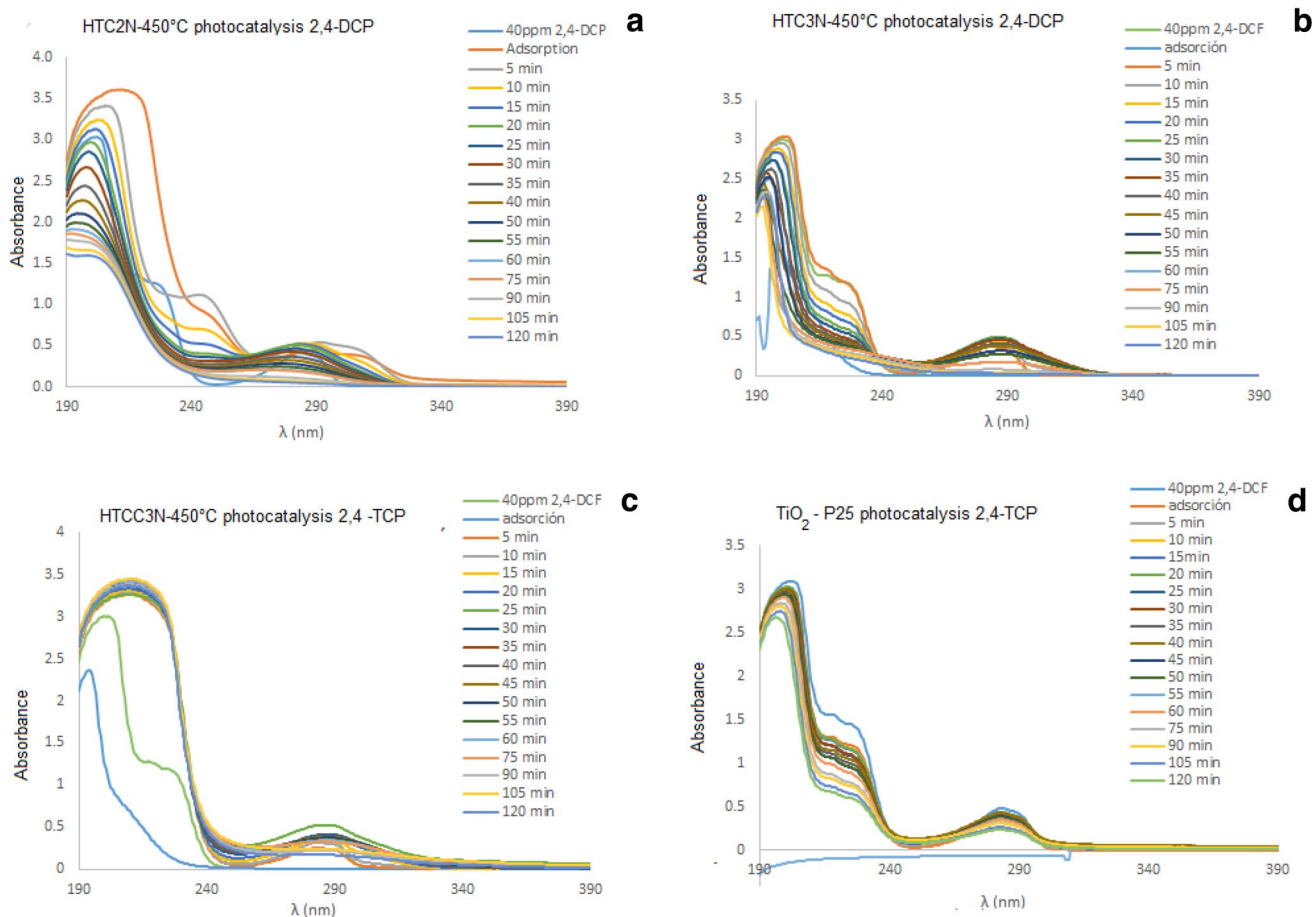


Fig. 8 UV–Vis spectra of the photocatalytic degradation of 2,4-dichlorophenol using layered double hydroxides HTC2N-450 °C, HTC3N-450 °C, HTCC3N-450 °C and TiO_2 P25-450 °C

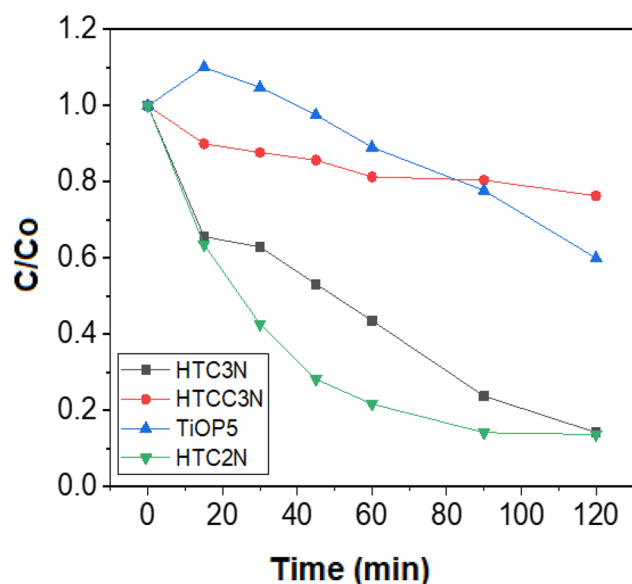


Fig. 9 Relative rate of photodegradation of 40 ppm of 2,4-dichlorophenol using layered double hydroxides HTC2N-450 °C, HTC3N-450 °C, HTCC3N-450 °C and TiO₂P25-450 °C

Figure 8a corresponds to the degradation spectra using the HTC2N-450 °C catalyst which shows how the bands decrease until their complete disappearance, associated with an almost complete degradation of the 2,4-dichlorophenol contaminant. Figure 8b shows the effect of degradation using the HTC3N-450 °C catalyst, being able to observe a good degradation activity, but being incomplete especially in the aromatic part of the contaminant. Figure 8c corresponds to degradation with the catalyst HTCC3N-450 °C which is very little active in the degradation of 2,4-Dichlorophenol. Finally, Fig. 8d corresponds to the degradation spectra of 2,4-dichlorophenol using TiO₂-450 °C as a reference photocatalyst. In this last spectrum the catalyst is not very active, especially in the shortest times of exposure to the contaminant.

Figure 9 shows the graph of the relative degradation rate of 40 ppm of 2,4-dichlorophenol with the different catalysts up to 120 min. The HTC2N catalyst activated at 450 °C shows a good degradability from the first 20 min by degrading 34% of the contaminant, continuing with the same speed up to 40 min degrading 72%, with the subsequent decrease in speed at 90 min to become constant and achieve degrading 84.5% of 2,4-dichlorophenol. On the other hand, the HTC3N-450 °C catalyst shows a good photocatalytic activity similar to those of HTC2N-450 °C during the first 20 min, but later its speed from 20 to 90 min degrading 75% of the contaminant, but with a speed increase of 90 at 120 min, with which it manages to degrade 83.5% of the contaminant, very similar to the HTC2N-450 °C catalyst. The above suggests that the Ni found in greater quantity in the

HTCN2-450 °C catalyst enhances the semiconductor capacity of double laminar hydroxides increasing the degradation rate of 2,4-Dichlorophenol. In the case of the HTC3N-450 °C catalyst, despite containing less Ni, once the solid is being photoinduced, both Ni and Al can contribute to photodegradation. With respect to the HTCC3N-450 °C catalyst, it shows a low photocatalytic activity, reaching 10% in the first 20 min, but drastically reducing its speed to reach only 60% at 60 min and at 22.5% at 120 min. The low activity of the HTCC3N-450 °C catalyst is attributed to the lack of generation of active sites due to the synthesis pH, as well as the combination of crystalline phases present in the solids at the time of activation. Finally, the degradation studies of 2,4-dichlorophenol using the TiO₂ reference catalyst, it can be seen that this shows low activity in the first 60 min where it degrades only 3% in the first 40 min, to later slightly increase its speed of degradation and reach 120.5% degradation after 120 min. Comparing the capacity of the reference catalyst with the double laminar hydroxides, it is found that only the HTCC3N-450 °C catalyst has a lower capacity, but the HTC2N-450 °C and HTC3N-450 °C catalysts exceed the catalyst in capacity and degradation rate by more than double at 120 min.

Figure 10 shows the degradation percentage of 2,4-dichlorophenol at 150 min where it can be seen that the catalyst with the highest degradability is HTC2N-450 °C with 94%, followed by HTC3N-450 °C catalyst with 86% and finally HTCC3N-450 °C with only 24%. The HTC3N-450 °C catalyst, showing a greater degradation capacity, the HTC3N-450 °C catalyst attributed to the higher Ni content, was selected to perform the study of the identification of degradation mechanism due to the effect of radicals and holes.

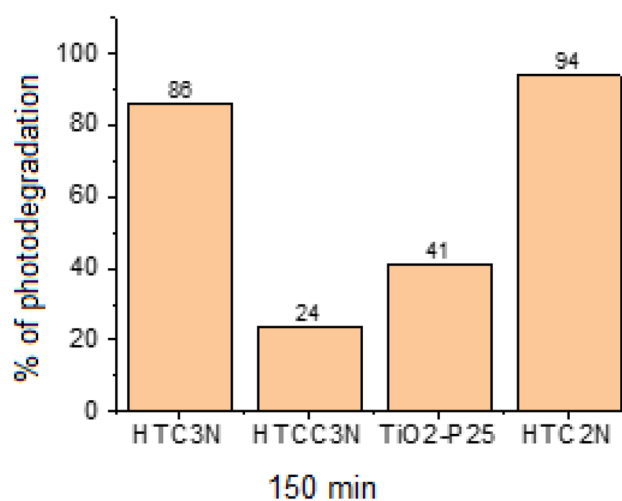


Fig. 10 Photodegradation of 2,4-dichlorophenol with different photocatalysts HTC2N-450 °C, HTC3N-450 °C, HTCC3N-450 °C and TiO₂P25 at 150 min

Fig. 11 Pseudo-first-order degradation kinetics for 40 ppm of 2,4-dichlorophenol with activated layered double hydroxides: HTC2N, HTC3N, HTCC3N and TiO₂-P25

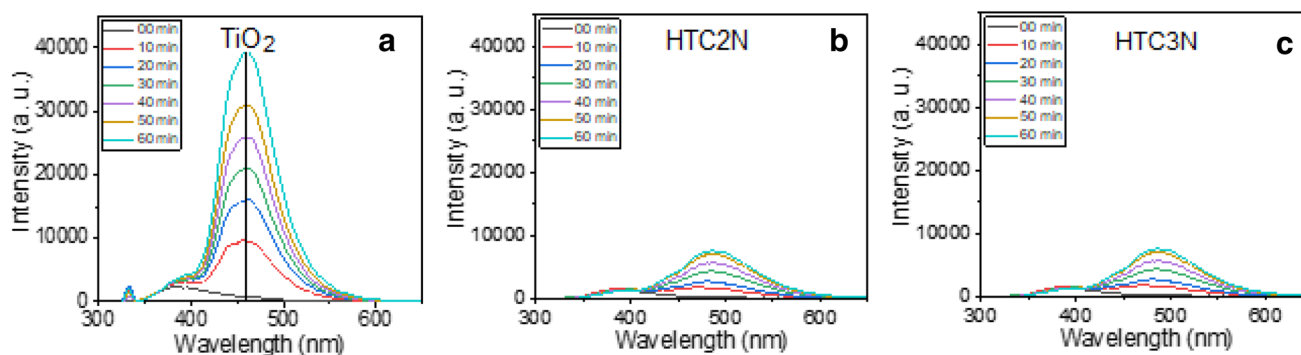
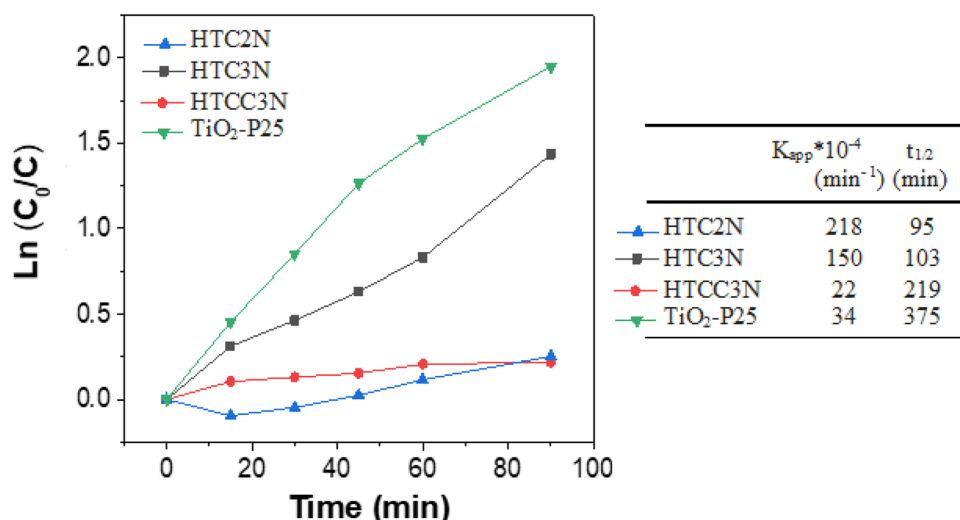


Fig. 12 Fluorescence spectra of the 2,4-dichlorophenol employed in the detection of OH[•] generate by TiO₂-P25-450 °C, HTC2N-450 °C and HTC3N-450 °C photocatalyst without air bubbling

3.7 Kinetic Model Adjustment Study

Figure 11 shows the adjustment of the kinetic model of the catalysts used in the photodegradation of 2,4-dichlorophenol. It is found that in all cases it corresponds to a degradation behavior of pseudo first order, adjusting to the kinetic model of Langmuir-Hinshelwood associated with steady state conditions.

Comparing the values of the apparent rate constant, the HTC2N catalyst presents a higher constant, associated with a higher rate of degradation, associated with a shorter half-life of elimination of the contaminant 2,4-dichlorophenol. On the other hand, the HTC3N catalyst presents a slightly less constant, but reaching the same degradation capacity of the HTC2N catalyst at 90 min. Finally, the HTCC3N catalyst has a much lower degradation capacity compared to the other two catalysts, with an apparent rate constant very close to TiO₂, which is why it is discarded as a useful catalyst in the degradation of 2,4-dichlorophenol.

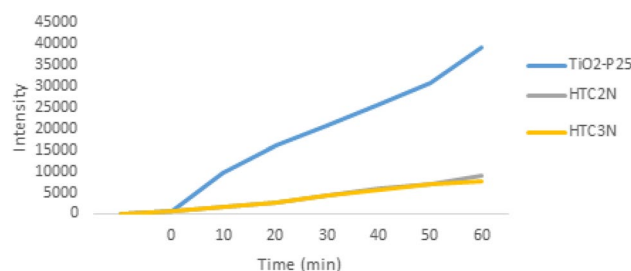


Fig. 13 Hydroxyl radical formation using the HTC2N, HTC3N and TiO₂-P25 catalysts

3.8 Hydroxyl and Superoxide Radical's Detection and Hole Trap Study

Figure 12 shows the identification of the formation of the OH[•] radicals with Fluorescence Spectroscopy by quantifying the formation of 7-hydroxycoumarin using the HTC2N-450

°C and HTC3N-450 °C catalysts and using as reference the TiO₂ 450 °C.

It is observed that the TiO₂ catalyst shows a rapid formation of radicals from the first 10 min, with a rapid evolution quadrupling the concentration at 60 min, which explains why the catalytic activity of TiO₂ begins until you have a high concentration of hydroxyl radicals to be able to start degrading to 2,4-dichlorophenol. On the other hand, the catalysts HTC2N and HTC3N show a very low production of hydroxyl radicals which increases slightly as the first 60 min pass, but without being significant for degradation, as it does not reach 25% of the concentration of radicals that it achieves produce TiO₂, as can be seen in Fig. 13 where the hydroxyl radical production isotherms are compared.

To determine the presence and influence of superoxide radicals on the degradation of 2,4-dichlorophenol, photodegradation tests were carried out in the absence of bubbling oxygen, that is, replacing the atmosphere by bubbling with nitrogen using HTC2N and HTC3N as catalysts. Figure 14 shows the absorption spectrum of the degradation process of 2,4-dichlorophenol in an atmosphere of N₂ (14a and 14c) compared to the absorption spectrum of the degradation process in an atmosphere of O₂ (Fig. 14b and d).

Comparing the a and b spectra of the HTC2N solid, it can be seen that the absorbance at 283 nm decreases, but the band at 210.5 nm practically remains constant until 120 min, indicating that partial dechlorination of the 2,4-Dichlorophenol molecule is occurring, but that the aromatic structure of phenol remains unchanged, implying a partial and insignificant degradation of the contaminating molecule in the absence of oxygen that allows the formation of superoxide radicals, compared to the high degradation capacity when oxygen is present. Regarding the behavior of the HTC3N catalyst, the spectrum c) and d) are very similar, with which it can be concluded that the activity of the superoxide radicals is not significant for the degradation process of 2,4-Dichlorophenol. Figure 15 shows the absorption spectra of 2,4-Dichlorophenol as a function of time during the photocatalytic degradation process of 2,4-Dichlorophenol in the presence of ammonium oxalate using HTC2N and HTC3N as catalysts.

It is observed that when ammonium oxalate is present as a sacrificial agent, the catalyst voids do not actively intervene in the degradation process of the pollutant, thus confirming that the voids are determining species in the photocatalytic mechanism of degradation of the 2,4-Dichlorophenol both for the dechlorination of the molecule and for the

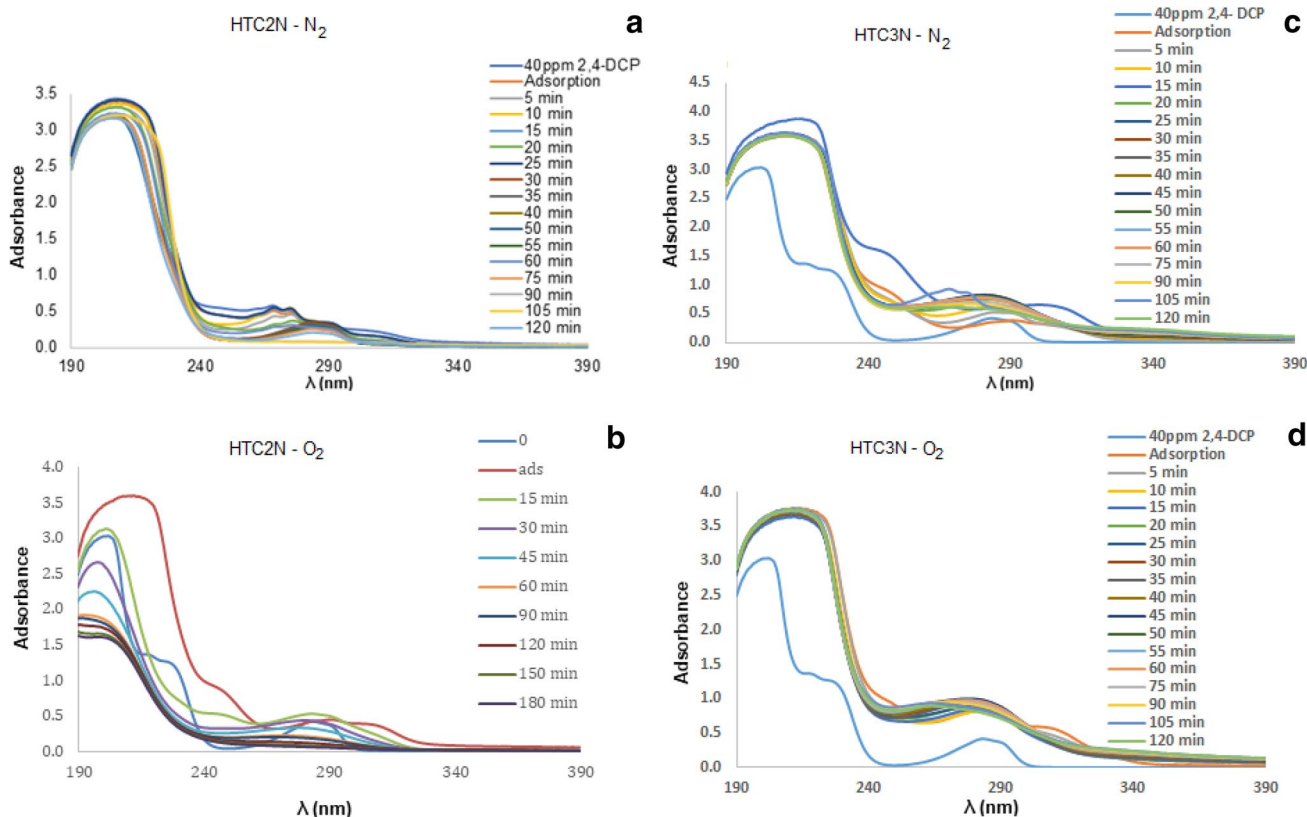


Fig. 14 Fluorescence spectra of the 2,4-Dichlorophenol employed in the detection of superoxide radicals generate by the HTC2N and HTC3N Photocatalysts, **a, c** in N₂ atmosphere, **b, d** in O₂ atmosphere

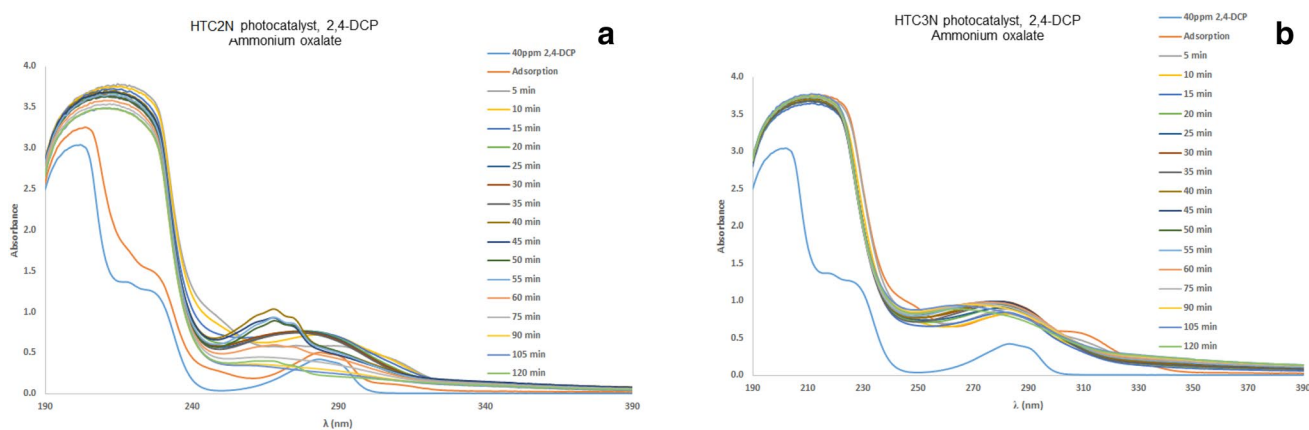


Fig. 15 Photocatalysis of 2,4-DCF with Ammonium Oxalate using as a catalyst **a** HTC2N and **b** HTC3N

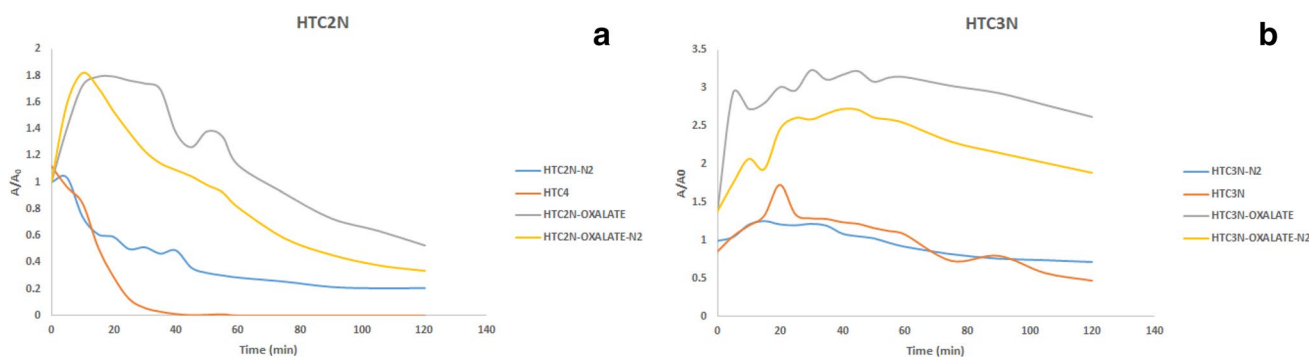


Fig. 16 Kinetics in the atmosphere of Oxygen, in the atmosphere of Nitrogen, in the Presence of Oxalate with oxygen and Oxalate with Nitrogen of the Catalysts **a** HTC2N and **b** HTC3N

degradation of the aromatic ring. Figure 16 makes it possible to compare the kinetic studies of the degradation of 2,4-Dichlorophenol using HTC2N and HTC3N as catalysts in an atmosphere of O₂, N₂, oxalate-O₂ and oxalate-N₂.

2,4-dichlorophenol in the presence of ammonium oxalate (HTC2N-oxalate) and in the presence of oxygen-free ammonium oxalate (HTC2N-oxalate-N₂) a considerable decrease in kinetics is observed, compared to the degradation reaction in the presence oxygen (HTC2N). Furthermore, an increase in the absorptivity coefficient can be observed in both processes, which implies an increase in intermediate products that, as there are no catalytically active voids, cannot be degraded. Comparing the effect of the atmosphere of O₂ and N₂ with oxalate, it is confirmed that the 2,4-Dichlorophenol molecule partially degrades in an oxygen atmosphere, forming a large number of intermediaries, but these cannot be degraded due to the lack of gaps, highlighting the importance of having the combination of superoxide radicals and gaps. For the HTC3N catalyst, the behavior with ammonium oxalate in both atmospheres also increases the absorptivity coefficient associated with the formation of intermediaries

which do not manage to be degraded within the first 120 min, unlike the HTC2N catalyst that does so after the first 60 min.

Performing the A/A₀ calculation at 120 min for the HTC2N catalyst, it is found that the superoxide radicals contribute 20% to the catalytic photodegradation, the voids contribute 50% and the hydroxyl radicals contribute 30%. For the HTC3N catalyst, it is found that the voids contribute 80%, hydroxyl radicals 15% and superoxide radicals 5% to catalytic photodegradation. This confirms the importance of having all the catalytically active species for the process to be carried out efficiently. The high contribution of the voids confirms the role of Ni as an active metal capable of releasing its electrons to the valence band and thus contributing to the generation of voids that activate the degradation activity together with the hydroxyl and superoxide radicals.

The previous results show that the HTC2N catalyst shows the highest activity significantly regulated by the activity of the voids, as well as the hydroxyl and superoxide radicals. This capacity is attributed both to the presence of the mixed oxide NiAl₂O₄, as well as the simple oxide NiO, with which

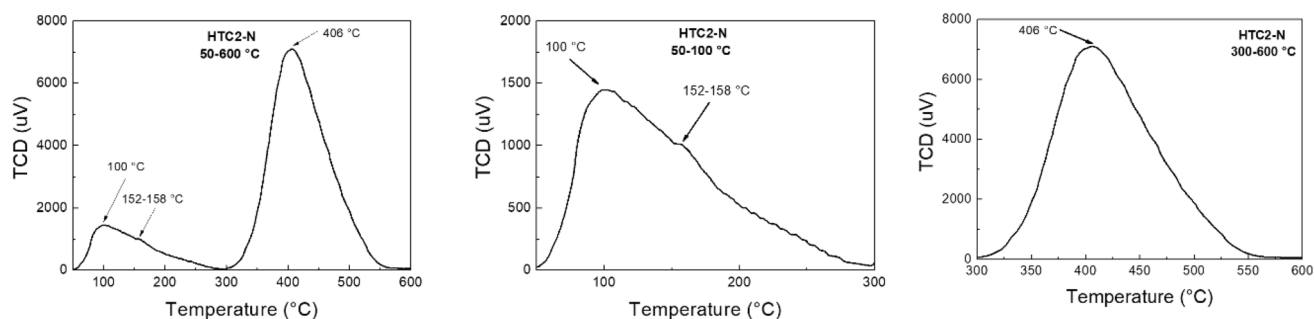


Fig. 17 TPD- CO_2 analysis for the HTC2N 450 °C

the relative rate of degradation is high, reaching a degradation of up to 94% in 150 min.

To complement the understanding of the photocatalytic properties of the HTC2N solid calcined at 450 °C, it was characterized by the techniques of TPD, SEM-EDS and TEM.

3.9 Analysis of Thermal Programmed Desorption (TPD) of CO_2

Figure 17 shows the analyzes of CO_2 TPD, for the HTC2N photocatalyst calcined at 450 °C. This technique was used to determine the density and strength of the basic centers in the mixed oxides derived from the layered double hydroxides. Three zones of desorption can be observed in the material. The first zone at 100 °C shows a desorption corresponding to 0.156 mmol CO_2/g active Ni/Al layered double hydroxide, this is weakly adsorbed CO_2 which is evacuated with mild heat treatments therefore the surface $-\text{CO}_2$ interaction is of

very low energy, continuing with the increase in temperature it maintains a continuous loss of CO_2 and a small near shoulder between 150 and 180 °C shows a slight increase in the loss of CO_2 (0.12 mmol / g) and possibly corresponds to CO_2 weakly chemisorbed [50], correspond to free carbonates bound to the material by a low energy bond, this low energy CO_2 desorption ends at the temperature of 300 °C. However, continuing with the route of the TPD at a temperature of 320 °C, a strong rise in the TPD begins, indicating an intense loss of chemisorbed CO_2 that reaches a maximum of 400 °C with an estimated loss of 1.26 mmol of CO_2/g catalytic converter and the final descent was 550 °C. This last intense loss at high temperatures is correlated with high energy basic sites (strong basic sites), that is, at these sites, CO_2 molecules are strongly chemisorbed, forming two bridged bonds of CO_2 with the surface of the photocatalyst, attributed to pairs of Lewis acid-base and low coordination surface O_2^- in which the CO_2 is linked in a monodentate form [51].

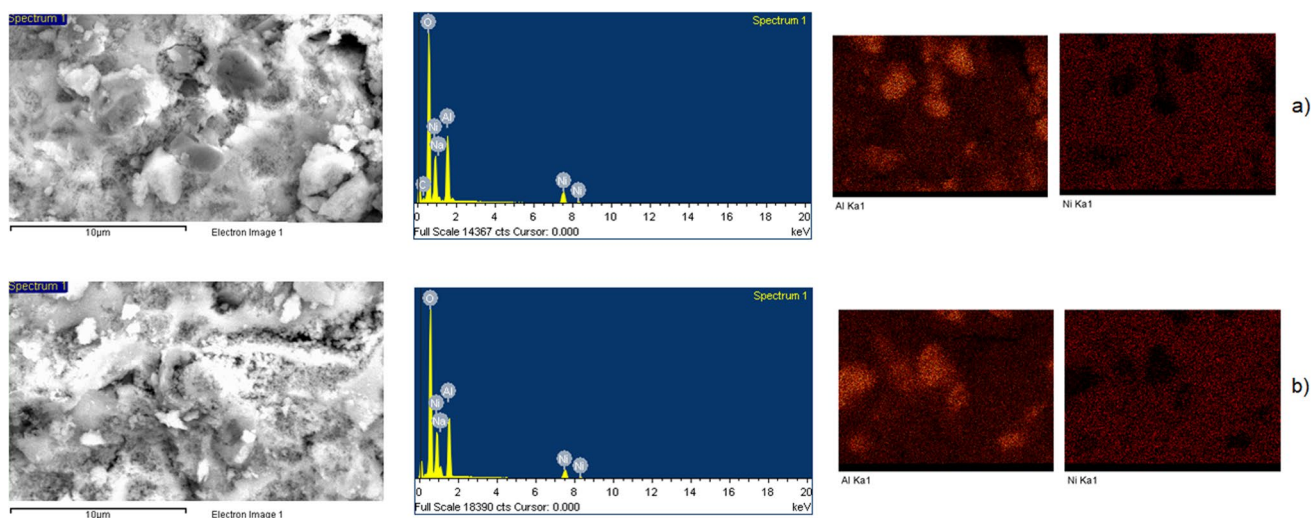


Fig. 18 SEM and EDS of HTC2N **a** untreated and **b** treated at 450 °C

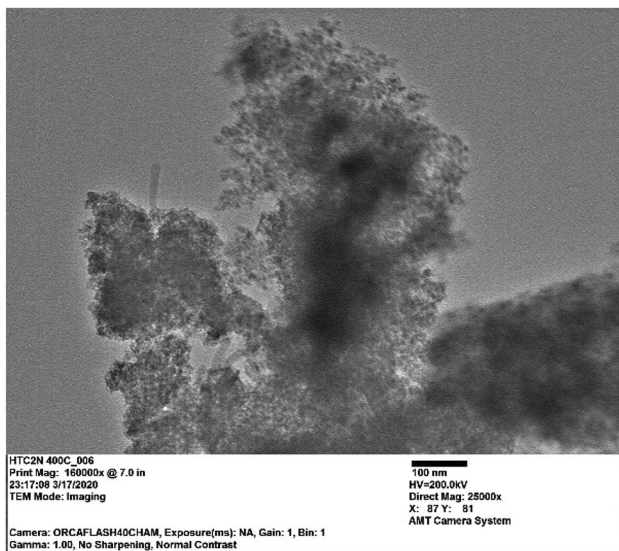


Fig. 19 TEM image of HTC2N a 450 °C

3.10 Scanning Electron Microscopy and X-ray Dispersive Energy Spectroscopy (SEM-EDS)

Figure 18 shows the SEM-EDS images of the HTC2N catalyst uncalcined (Fig. 18a) and calcined at 450 °C (Fig. 18b) [41, 52]. Comparing the SEM images of solid before and after calcining it at 450 °C, both solids have particles of variable sizes that form micron-sized aggregates. Specifically, the calcined solid has a greater quantity of finely dispersed individual nano-sized particles on the solid in the bulk, which favors the exposure of the catalytically active sites on the surface of the catalyst. The elemental mapping of Al and Ni shows a homogeneous dispersion of both elements in all particles of the solid without calcining and after calcination, but increasing the density of ions on the surface when the solid is calcined due to dehydration, decarbonation and dehydroxylation of the precursor.

3.11 Transmission Electron Microscopy (TEM)

In the TEM image of the Ni/Al layered double hydroxides calcined at 450 °C, isolated nanoparticles with sizes smaller than 10 nm are observed [52]. These nanoparticles agglomerate to form clusters as seen in Fig. 19. The elemental quantification for the determination of the Ni/Al molar ratio confirms that the ratio of the metal ions is $11.15/5.58 = 1.999 = 2.0$.

4 Conclusions

The results of this study indicated that by calcining the metallic ratio Ni/Al=2 and 3 layered double hydroxides synthesized at a pH of 11.5 at 450 °C, catalytically active materials are obtained to be used efficiently in the degradation of 2,4-dichlorophenol. The catalyst that achieves a degradation capacity of up to 94% in 150 min is the one that contains a Ni/Al=2 metal ratio in a solution of 2 mg of catalyst/mL of 40 ppm solution of 2,4-dichlorophenol. Kinetic studies found that the degradation process follows a pseudo-first order process with apparent rate constants of up to $218 \times 10^{-4} \text{ s}^{-1}$ and half-life times of 95 min. The degradation process of 2,4-dichlorophenol is carried out through a degradation mechanism combined by the action of superoxide radicals with 20%, holes with 50% and hydroxyl radicals with 30%. These oxidation-reduction species are present in the catalyst which is a mixture of nanoparticles with strong basic sites. For the HTC3N catalyst, a lower degradation capacity is reached, with values of 86%, as a result of the effect of the voids that provide the highest catalytic activity with 80%, hydroxyl radicals 15% and superoxide radicals 5% due to the presence of amorphous NiAl₂O₄ nanoparticles mixed with NiO nanoparticles. For both catalysts the catalytic activity is not attributed to the memory effect since the solid is not rebuilt during the degradation process, but the catalytic activity is attributed to the crystalline and amorphous species of the metal oxides that contain Ni. The reason why the Ni/Al=2 ratio catalyst is more active in the degradation of 2,4-dichlorophenol, compared to the Ni/Al=3 catalyst, is that Ni, being a transition metal with properties Strong reducing agent favors the semiconductor capacity of the catalysts with NiO-NiAl₂O₄ mixtures than different metallic species, and being in a greater quantity in the solid of Ni/Al ratio=2, achieving to generate a crystalline network with a band energy 2.89 eV is prohibited, below the 3.2 energy that TiO₂ has. The physicochemical characterization of the catalysts allowed to check the effect of crystallinity, as well as the distribution of Ni/Al metals within the crystalline structures that form when calcined at 450 °C associated with the phase transition and activation temperature. The catalyst that showed a poor degradation capacity was the Ni/Al=3 ratio but that was obtained at a very basic synthesis pH of 12.6, which affected its structural and thermal evolution properties, confirming the director effect of the synthesis conditions on the generation of catalytically active sites.

Acknowledgements The authors thank CONACYT, UAM-I and UG for your support and funding. Additionally, we thank Dr. Mirella Gutiérrez A. from UAM-A and Dr. Raul Pérez-Hernandez from ININ for their scientific-technological support.

Compliance with Ethical Standards

Conflict of interest The authors declare no conflict of interest.

References

- Nugen S, Baeumner HJ (2008) Trends and opportunities in food pathogen detection. *Anal Bioanal Chem* 391:451–454
- Nakata K, Fujishima A (2012) TiO₂ photocatalysis: design and applications. *J Photochem Photobiol C* 13:169–189. <https://doi.org/10.1016/j.jphotochemrev.2012.06.001>
- Jack R, Ayoko G, Adebajo M, Frost R (2015) A review of iron species for visible-light photocatalytic water purification. *Environ Sci Pollut Res* 22:7439–7449. <https://doi.org/10.1007/s11356-015-4346-5>
- Chong MN, Jin B, Chow CWK, Saint C (2010) Recent developments in photocatalytic water treatment technology: a review. *Water Res* 44:2997–3027
- Fajrina N, Tahir M (2019) A critical review in strategies to improve photocatalytic water splitting towards hydrogen production. *Int J Hydrogen Energ* 44:540–577
- Athanasekou CP, Likodimos V, Falaras P (2018) Recent developments of TiO₂ photocatalysis involving advanced oxidation and reduction reactions in water. *J Environ Chem Eng* 6(6):7386–7394. <https://doi.org/10.1016/j.jece.2018.07.026>
- Fujishima A, Honda K (1972) Electrochemical photolysis of water at a semiconductor electrode. *Nature* 238:37–38
- Zhao C, Liu L, Rao G, Zhao H, Wang L, Xu J, Li Y (2015) Synthesis of novel MgAl layered double oxide grafted TiO₂ cuboids and their photocatalytic activity on CO₂ reduction with water vapor. *Catal Sci Technol* 5:3288. <https://doi.org/10.1039/c5cy00216h>
- Choquette-Labbé M, Shewa WA, Lalman JA, Shanmugam SR (2014) Photocatalytic degradation of phenol and phenol derivatives using a nano-TiO₂ catalyst: integrating quantitative and qualitative factors using response surface methodology. *Water* 6:1785–1806. <https://doi.org/10.3390/w6061785>
- Abdel-Maksoud Y, Imam E, Ramadan A (2016) TiO₂ solar photocatalytic reactor systems: selection of reactor design for scale-up and commercialization: analytical. *Rev Catal* 6:138. <https://doi.org/10.3390/catal6090138>
- Österlund L, Mattsson A, Brischetto M, Byberg JJ, Stefanov BI, Ji YX, Niklasson GA (2018) Spectral selective solar light enhanced photocatalysis: TiO₂/TiAlN bilayer films. *Top Catal* 61:1607–1614. <https://doi.org/10.1007/s11244-018-1011-5>
- Chen H, Liu XY, Hao XD, Zhang YX (2016) Facile biphasic synthesis of TiO₂-MnO₂ nanocomposites for photocatalysis. *Ceram Int* 42:19425–19428. <https://doi.org/10.1016/j.ceramint.2016.08.160>
- Zhou P, Le V, Xie YJ, Xu J (2017) Studies on facile synthesis and properties of mesoporous CdS/TiO₂ composite for photocatalysis applications. *J Alloy Compd* 692:170–177. <https://doi.org/10.1016/j.jallcom.2016.09.039>
- Mazierski P, Mikolajczyk A, Bajorowicz B, Malankowska A, Zaleska-Medynska A, Nadolna J (2018) The role of lanthanides in TiO₂-based photocatalysis: a review. *Appl Catal B* 233:301–317. <https://doi.org/10.1016/j.apcatb.2018.04.019>
- Zhou P, Le Z, Xie Y, Fang J, Xu J (2017) Studies on facile synthesis and properties of mesoporous CdS/TiO₂ composite for photocatalysis applications. *J Alloy Compd* 692:170–177. <https://doi.org/10.1016/j.jallcom.2016.09.039>
- Marchelek M, Grabowska E, Klimczuk T, Lisowski W, Mazierski P, Zaleska-Medynska A (2018) Visible light photocatalysis employing TiO₂/SrTiO₃-BiOI composites: surface properties and photoexcitation mechanism. *Mol Catal* 452:154–166. <https://doi.org/10.1016/j.mcat.2018.04.006>
- Chung SG, Chang YS, Choi JW, Baek KY, Hong SW, Yun ST, Lee SH (2013) Photocatalytic degradation of chlorophenols using star block copolymers: removal efficiency, by-products and toxicity of catalyst. *Chem Eng J* 215–216:921–928. <https://doi.org/10.1016/j.cej.2012.11.070>
- Jimenez-Tototzintle M, Jales I, da Silva S, Guimaraes PR, Mendes E (2018) Removal of contaminants of emerging concern (CECs) and antibiotic resistant bacteria in urban wastewater using UVA/TiO₂/H₂O₂ photocatalysis. *Chemosphere* 210:449–457. <https://doi.org/10.1016/j.chemosphere.2018.07.036>
- Irawaty W, Soetaredjo FE, Ayucitra A (2014) Understanding the relationship between organic structure and mineralization rate of TiO₂-mediated photocatalysis. *Procedia Chem* 9:131–138
- Al-Mamun MR, Kader S, Islam MS, Khan MZH (2019) Photocatalytic activity improvement and application of UV-TiO₂ photocatalysis in textile wastewater treatment: a review. *J Environ Chem Eng* 7:103248. <https://doi.org/10.1016/j.jece.2019.103248>
- Hu X, Hu X, Peng Q, Zhou L, Tan X, Jiang L, Tang C, Wang H, Liu S, Wang Y, Ning Z (2020) Mechanisms underlying the photocatalytic degradation pathway of ciprofloxacin with heterogeneous TiO₂. *Chem Eng J* 380:122366. <https://doi.org/10.1016/j.cej.2019.122366>
- Holcombe GW, Phipps GL, Fiandt JT (1982) Effects of phenol, 2,4-dimethylphenol, 2,4-dichlorophenol, and pentachlorophenol on embryo larval, and early-juvenile Fathead Minnows (*Pimephales promelas*). *Arch Environ Contam Toxicol* 11:73–78
- Boyd EM, Killham K, Meharg AA (2001) Toxicity of mono-, di- and tri-chlorophenols to lux marked terrestrial bacteria, *Burkholderia* species Rasc c2 and *Pseudomonas fluorescens*. *Chemosphere* 43:157–166
- Zheng D, Jiao H, Zhong H, Qiu J, Yan X, Duan Q, Chai L (2018) Chlorophenols in marine organisms from the southern coast of Hangzhou Bay, China, and an assessment of risks posed to human health. *J Oceanol Limnol* 36(3):726–737. <https://doi.org/10.1007/s00343-018-7039-3>
- Kukkonen JVK (2002) Lethal body residue of chlorophenols and mixtures of chlorophenols in benthic organisms. *Arch Environ Contam Toxicol* 43:214–220. <https://doi.org/10.1007/s00244-002-1174-7>
- Yu J, Wang T, Rtimi S (2019) Magnetically separable TiO₂/FeO_x/POM accelerating the photocatalytic removal of the emerging endocrine disruptor: 2,4-dichlorophenol. *Appl Catal B* 254:66–75. <https://doi.org/10.1016/j.apcatb.2019.04.088>
- Ruan X, Liu H, Wang J, Zhao D, Fan X (2019) A new insight into the main mechanism of 2,4-dichlorophenol dechlorination by Fe/Ni nanoparticles. *Sci Total Environ* 697:133996. <https://doi.org/10.1016/j.scitotenv.2019.133996>
- Diao ZH, Yan L, Dong FX, Qian W, Deng QH, Kong LJ, Yang JW, Lei ZX, Du JJ, Chu W (2020) Synergism with Cd(II) immobilization in a contaminated soil. *Chem Eng J* 379:122313. <https://doi.org/10.1016/j.cej.2019.122313>
- Diao XH, Yan L, Dong FX, Qian W, Deng QH, Kong LJ, Yang JW, Lei ZX, Du JJ, Chu W (2009) ZnO/Mg–Al layered double hydroxides as strongly adsorptive photocatalysts. *Res Chem Intermed* 35:685–692. <https://doi.org/10.1007/s11164-009-0094-9>
- Wu SZ, Li N, Zhang WD (2014) Attachment of ZnO nanoparticles onto layered double hydroxides microspheres for high performance photocatalysis. *J Porous Mater* 21:157–164. <https://doi.org/10.1007/s10934-013-9760-9>

31. Cavani F, Trifiro F, Vaccari A (1992) Hydrotalcite-type anionic clays: preparation, properties and applications. *Catal Today* 11:173–301
32. Roelofs JCAA, Bokhoven JA, Dillen AJ, Jong KP (2002) The thermal decomposition of Mg ± Al hydrotalcites: effects of inter-layer anions and characteristics of the final structure. *Chem Eur J* 8:5571–5579
33. Yahyaoui R, Sanchez PE, Pérez LA, Nahdi K, Criado JM (2018) Synthesis, characterization and combined kinetic analysis of thermal decomposition of hydrotalcite (Mg₆Al₂(OH)₁₆CO₃·4H₂O). *Thermochim Acta* 667:177–184. <https://doi.org/10.1016/j.tca.2018.07.025>
34. Nguyen HKD, Nguyen HV, Nguyen VA (2018) Effect of synthetic conditions on the structure of mesoporous Mg-Al-Co hydrotalcite. *J Mol Struct* 1171:25–32. <https://doi.org/10.1016/j.molstruc.2018.05.087>
35. Zhang D, Zhao G, Yu J, Yan T, Zhu M, Jiao F (2016) Thermodynamic and kinetic studies of effective adsorption of 2,4,6-trichlorophenol onto calcined Mg/Al-CO₃ layered double hydroxide. *J Wuhan Univ Technol* 31:1211–1218. <https://doi.org/10.1007/s11595-016-1514-5>
36. Yang B, Liu J, Liu Z, Wang Y, Cai J, Peng L (2019) Preparation of chitosan/Co-Fe-layered double hydroxides and its performance for removing 2,4-dichlorophenol. *Environ Sci Pollut Res* 26:3814–3822. <https://doi.org/10.1007/s11356-018-3886-x>
37. Zhou S, Li C, Zhao G, Liu L, Yu J, Jiang X, Jiao F (2019) Heterogeneous co-activation of peroxymonosulfate by CuCoFe calcined layered double hydroxides and ultraviolet irradiation for the efficient removal of p-nitrophenol. *J Mater Sci Mater Electron* 30:19009–19019. <https://doi.org/10.1007/s10854-019-02258-0>
38. Prasad C, Tang H, Liu W (2018) Magnetic Fe₃O₄ based layered double hydroxides (LDHs) nanocomposites (Fe₃O₄/LDHs): recent review of progress in synthesis, properties and applications. *J Nanostruct Chem* 8:393–412. <https://doi.org/10.1007/s40097-018-0289-y>
39. Zheng K, Song Y, Wang X, Li X, Mao X, Wang D (2019) Understanding the electrode reaction process of dechlorination of 2,4-dichlorophenol over Ni/Fe nanoparticles: effect of pH and 2,4-dichlorophenol concentration. *J Environ Sci* 84:13–20. <https://doi.org/10.1016/j.jes.2019.01.012>
40. Yang B, Cai J, Wei S, Nie N, Liu J (2020) Preparation of chitosan/NiFe-layered double hydroxides composites and its fenton-like catalytic oxidation of phenolic compounds. *J Polym Environ* 28:343–353. <https://doi.org/10.1007/s10924-019-01614-9>
41. Alzhrani G, Ahmed NS, Aazam ES, Saleh TS, Mokhtar M (2019) Novel efficient Pd-free Ni-layered double hydroxide catalysts for a Suzuki C-C coupling reaction. *Chem Select*. <https://doi.org/10.1002/slct.201900890>
42. Tsai KJ, Ni CS, Chen HY, Huang JH (2020) Single-walled carbon nanotubes/Ni-Co-Mn layered double hydroxide nanohybrids as electrode materials for high-performance hybrid energy storage devices. *J Power Sources* 4541:2020227912. <https://doi.org/10.1016/j.jpowsour.2020.227912>
43. Klemkaite K, Prosycevas I, Taraskevicius R, Khinsky A, Kareiva A (2011) Synthesis and characterization of layered double hydroxides with different cations (Mg, Co, Ni, Al), decomposition and reformation of mixed metal oxides to layered structure. *Cent Eur J Chem* 9(2):275–282. <https://doi.org/10.2478/s11532-011-0007-9>
44. Belskaya OB, Leonteva NN, Gulyaeva TI, Cherepanova SV, Talzi VP, Drozdov VA, Likholobov VA (2013) Influence of a doubly charged cation nature on the formation and properties of mixed oxides MAIOx (M = Mg²⁺, Zn²⁺, Ni²⁺) obtained from the layered hydroxide precursors. *Russ Chem Bull* 62(11):2349–2361
45. Zhao L, Li X, Hao CE, Raston CL (2012) SO₂ adsorption and transformation on calcined NiAl hydrotalcite-like compounds surfaces: An in situ FTIR and DFT study. *Appl Catal B* 117–118:339. <https://doi.org/10.1016/j.apcatb.2012.01.034>
46. Mardani HR (2017) (Cu/Ni)-Al layered double hydroxides@Fe₃O₄ as efficient magnetic nanocomposite photocatalyst for visible-light degradation of methylene blue. *Res Chem Intermed* 43:5795–5810. <https://doi.org/10.1007/s11164-017-2963-y>
47. Foruzin LJ, Rezvani Z, Nejati K (2018) Preparation of two-color photoluminescence emission based on azo dye-layered double hydroxide systems and controlling photoluminescence properties of Allura Red AC. *J Iran Chem Soc* 15:2649–2658. <https://doi.org/10.1007/s13738-018-1453-5>
48. Castañeda C, Tzompantzi F, Gómez R, Rojas H (2016) Enhanced photocatalytic degradation of 4-chlorophenol and 2,4-dichlorophenol on in situ phosphated sol-gel TiO₂. *J Chem Technol Biotechnol* 91:2170–2178. <https://doi.org/10.1002/jctb.4943>
49. Coenen K, Gallucci F, Mezari B, Hensen E, Annaland M (2018) An in-situ IR study on the adsorption of CO₂ and H₂O on hydrotalcites. *J CO₂ Util* 24:228–239
50. Wierzbicki D, Baran R, Dębek R, Motak M, Gálvez ME, Grzybek T, Da Costa P, Glatzel P (2018) Examination of the influence of La promotion on Ni state in hydrotalcite-derived catalysts under CO₂ methanation reaction conditions: operando X-ray absorption and emission spectroscopy investigation. *Appl Catal B* 232(15):409–419. <https://doi.org/10.1016/j.apcatb.2018.03.089>
51. Wang W, Xu Z, Guo Z, Jiang C, Chu W (2015) Layered double hydroxide and related catalysts for hydrogen production and a biorefinery. *Chin J Catal* 36:139–147. [https://doi.org/10.1016/S1872-2067\(14\)60229-1](https://doi.org/10.1016/S1872-2067(14)60229-1)
52. Lu B, Zhuang J, Du J, Gu F, Xu G, Zhong Z, Liu Q, Su F (2019) Highly dispersed Ni nanocatalysts derived from NiMnAl-hydrotalcites as high-performing catalyst for low-temperature syngas methanation. *Catalysts* 9:282. <https://doi.org/10.3390/catal9030282>

Publisher's Note Springer Nature remains neutral with regard to jurisdictional claims in published maps and institutional affiliations.